Structural and Functional Studies on DHC, the Diheme Cytochrome *c* from *Rhodobacter sphaeroides*, and Its Interaction with SHP, the *sphaeroides* Heme Protein[†,‡]

Helen R. Gibson,[§] Christopher G. Mowat,[§,||] Caroline S. Miles,[||] Bor-Ran Li,[§] David Leys,[⊥] Graeme A. Reid,[||] and Stephen K. Chapman*[,§]

School of Chemistry, University of Edinburgh, West Mains Road, Edinburgh EH9 3JJ, U.K., Institute of Structural and Molecular Biology, University of Edinburgh, Mayfield Road, Edinburgh EH9 3JR, U.K., and Faculty of Life Sciences, Manchester Interdisciplinary Biocentre, c/o Jackson's Mill, University of Manchester, P.O. Box 88, Manchester M60 1QD, U.K.

Received February 10, 2006; Revised Manuscript Received March 28, 2006

ABSTRACT: The diheme cytochrome *c* (DHC) from *Rhodobacter sphaeroides* is a soluble protein with a mass of 16 kDa that represents a new class of *c*-type cytochrome [Vandenberghe, I., et al. (1998) *Biochemistry 37*, 13075−13081]. The gene encoding DHC is associated with another encoding a cytochrome known as SHP (*sphaeroides* heme protein). It is believed that DHC is the electron donor for SHP, which is known to bind oxygen. To gain further insight into the properties and role of DHC, we have carried out structure−function studies on the protein and examined its interaction with SHP. The crystal structures of native and recombinant DHC have been determined to resolutions of 1.85 and 2.0 Å, respectively. The structures show that DHC folds into two distinct domains each containing one heme. While the N-terminal domain is a class I cytochrome *c*, the C-terminal domain shows no similarity to any existing structures and thus constitutes a novel cytochrome *c* structural motif. The shortest, edge-to-edge, distance between the heme groups is 10.2 Å, and this distance is bridged by Tyr31, thus ensuring fast internal electron transfer. DHC binds strongly to its proposed physiological partner, SHP ($K_d = 0.26\ \mu$M in 10 mM HEPES at pH 7.2 and 25 °C). However, at higher salt concentrations, the binding becomes much weaker, indicating the importance of electrostatic interactions. DHC is also very efficient in electron transfer to SHP with a second-order rate constant of $1.8 \times 10^7\ M^{-1}\ s^{-1}$ (at pH 7.2, 10 °C, and $I = 500$ mM). The reduction potentials of DHC and SHP are also suitably ordered for a favorable reaction with the hemes of DHC showing potentials of −310 and −240 mV, respectively, and that for SHP being −105 mV. These potentials are unaltered upon complex formation.

The purple photosynthetic bacterium *Rhodobacter sphaeroides* produces five soluble *c*-type cytochromes and one *b*-type during phototrophic growth: cytochromes c_2, c', $c_{551.5}$, c_{554}, and b_{558} and an oxygen binding *c*-type protein (*1*). Of these, cytochrome $c_{551.5}$ has been renamed DHC[1] (diheme cytochrome *c*) and the oxygen binding protein designated SHP (*sphaeroides* heme protein).

SHP has a molecular mass of 12.5 kDa, contains a single high-spin heme, and has been demonstrated to transiently bind O_2 during autoxidation (*1*). SHP is not homologous to any of the other known gas-binding heme proteins such as the globins, FixL (*2*), CooA (*3*), or sGC (*4*). The crystal structures of the oxidized, reduced, cyanide-bound, and NO-bound forms of SHP have been determined (*5*). The structure of the oxidized protein shows SHP to be a member of the family of class I cytochromes *c* with a number of interesting features. In SHP, the *c*-type heme is axially ligated by His47 and Asn88. The occurrence of an amide group as a ligand to the heme iron is unique to SHP. Upon reduction of SHP, Asn88 is no longer ligated to the heme, leaving the amide group 3.0 Å from the pentacoordinate Fe(II) and making the iron available for the binding of small molecules such as O_2, NO, and CN^-. In addition, a disulfide bond between Cys89 and Cys97, along with a salt bridge between Arg95 and Glu101, serves to restrict access of large molecules to the heme. The oxidized, cyanide-bound crystal structure of SHP shows that cyanide binding causes a deformation of the cavity on the distal side of the heme in contrast to the reduced NO-bound structure.

[†] This work was supported by the Leverhulme Trust. D.L. is a Royal Society University Research Fellow and an EMBO Young Investigator. We thank ESRF Grenoble and SRS Daresbury for the use of synchrotron facilities.

[‡] Structure factors and model coordinates have been deposited with the Protein Data Bank (entry 2FWT for *R. sphaeroides* purified DHC and entry 2FW5 for recombinant DHC).

* To whom correspondence should be addressed: School of Chemistry, University of Edinburgh, West Mains Road, Edinburgh EH9 3JJ, U.K. E-mail: S.K.Chapman@ed.ac.uk. Fax and phone: (44) 131 650 4760.

[§] School of Chemistry, University of Edinburgh.

[||] Institute of Structural and Molecular Biology, University of Edinburgh.

[⊥] University of Manchester.

[1] Abbreviations: DHC, diheme cytochrome *c*; SHP, *sphaeroides* heme protein; PMSF, phenylmethanesulfonyl fluoride; EDTA, ethylenediaminetetraacetic acid; MES, 2-(*N*-morpholino)ethanesulfonic acid; MAD, multiwavelength anomalous dispersion; OTTLE, optically transparent thin layer electrode; SHE, standard hydrogen electrode.

10.1021/bi060288q CCC: $33.50
Published on Web 04/26/2006

Genes encoding SHP homologues have been detected in a wide variety of proteobacteria, including the metal oxide-reducing bacterium *Shewanella oneidensis* MR-1 (*6*), the magnetite synthesising bacteria *Magnetospirillum magnetotacticum* and *Magnetococcus* sp. MC-1 (*7*), *Burkholderia vietnamiensis* G4 (*8*), *Thiobacillus denitrificans* ATCC 25259, *Rhodoferax ferrireducens* DSM 15236, *Rhodospirillum rubrum* ATCC 11170 (*7*), *Dechloromonas aromatica* RCB (*9*), *Azoarcus* sp. EbN1 (*7*), and the pathogen *Campylobacter fetus* (*10*). The bacterium *Methylophilus methylotrophus* produces a cytochrome *c*″ which is 32% identical to SHP. Sequence alignments indicate that the disulfide bridge mentioned above is conserved in all SHP homologues. Asn88 is predominantly conserved as the sixth heme ligand but is replaced by Asp in *M. magnetotacticum* and *Rh. rubrum* SHP and by a second histidine residue in the *Me. methylotrophus* cytochrome *c*″. Reduction of the cytochrome *c*″ results in the loss of this ligand to leave a pentacoordinate heme iron. Consequently, the heme iron becomes high-spin (histidine being a strong field ligand and the oxidized protein containing low-spin heme), and there is a marked increase in the pK_a of the histidine that is released. Neither of these effects is observed in SHP because asparagine is neither readily ionizable nor a strong field ligand.

The physiological function of SHP is unknown, but the known genetic organization indicates that it is likely to be a component of a conserved electron transfer pathway. The SHP coding sequence is, wherever it occurs, immediately adjacent to a reading frame encoding a diheme cytochrome *c* homologous to DHC in *R. sphaeroides*. DHC has a molecular mass of 16 kDa, and the amino acid sequence indicates that this protein represents a new class of *c*-type cytochromes (*11*). The suggestion of a conserved genetic link between DHC and SHP has led to the idea that DHC may be the physiological electron donor for SHP. A membrane-bound cytochrome *b* found in the same gene cluster is likely to transfer electrons from the quinone pool to DHC, and on to SHP which may function as the terminal member of a novel respiratory pathway. In this paper, we report the crystal structure of DHC in two crystal forms and investigate the interaction between SHP and DHC.

MATERIALS AND METHODS

DNA Manipulation, Strains, Media, and Growth. pMc519 (*12*) was used to express the SHP protein from *R. sphaeroides* 2.4.1 in *Escherichia coli*. This plasmid, which confers both ampicillin and chloramphenicol resistances, contains DNA encoding the signal sequence of the *E. coli* alkaline phosphatase (sPhoA) downstream of a *tac* promoter and ribosome binding site. DNA encoding the mature SHP was amplified by PCR with *Xmn*I and *Sph*I restriction endonuclease sites incorporated at the 5′ and 3′ ends, respectively. pMc519 was digested with *Kpn*I and then blunt-ended prior to subsequent digestion with *Sph*I. The PCR product was digested with *Xmn*I and *Sph*I and then ligated with the vector fragment described above. This generated a fusion of the DNA encoding the mature SHP, incorporating an upstream six-base ATTTCA segment (encoding an isoleucine and a glycine amino acid residue), with that of the sPhoA. The resulting construct, pMc519SHP, was sequenced to ascertain that the fusion was in-frame and that no mutations had occurred.

For expression in *E. coli*, strain MC1061 was cotransformed with pMc519SHP and pEC86-Km^r, a version of pEC86 (*13*) in which the chloramphenicol resistance has been replaced with kanamycin (*14*). The pEC86 plasmid contains the cytochrome *c* maturation genes necessary for expression of *c*-type cytochromes in *E. coli*. The SHP expression strain was grown in Luria-Bertani (LB) medium supplemented with carbenicillin (100 μg/mL) and kanamycin (50 μg/mL) in a shaker incubator at 120 rpm and 37 °C for 8 h (until the OD_{600} reached ≈1.0). Cells were then induced with 1 mM IPTG and incubated overnight (approximately 16 h).

For DHC production, DNA encoding the mature protein from *R. sphaeroides* 2.4.1 was amplified by PCR with *Nae*I and *Hin*dIII restriction endonuclease sites being introduced at the 5′ and 3′ ends. Following digestion, the PCR fragment was cloned into plasmid pT10sOmpArPDI, thereby fusing the vector-encoded signal peptide of the bacterial outer-membrane protein A (sOmpA) to DHC. DNA encoding the fusion was then excised from the construct as an *Xba*I−*Hin*dIII fragment and subcloned into the pLPPsOmpArPDI expression vector (*15*). Subsequent sequence analysis confirmed that no mutations were present and that the fusion was in-frame. To avoid proteolysis of DHC, it was expressed in *E. coli* using the *degP*$^-$ strain (a kind gift from L. Thöny-Meyer, Mikrobiologisches Institut, ETH Zentrum, Zürich, Switzerland) and was cotransformed with pLPPsOmpADHC and pEC86.

The DHC expression strain was grown in Luria-Bertani (LB) medium supplemented with carbenicillin (100 μg/mL) and chloramphenicol (25 μg/mL) in a shaker incubator at 120 rpm and 37 °C. Expression was induced with 1 mM IPTG at an OD_{600} of ≈0.5, and cells were incubated for a further 4 h prior to being harvested by centrifugation.

Protein Purification. Purification of DHC was carried out as follows. *E. coli* cells expressing DHC were suspended in 100 mM Tris-HCl (pH 7.5) and disrupted by sonication, and cell debris was removed by centrifugation (18000*g* for 30 min). The supernatant was loaded directly onto a Q-Sepharose anion exchange column pre-equilibrated with the same buffer. Recombinant DHC was observed to bind tightly to the column, which was then developed by application of a 0 to 500 mM KCl gradient. Fractions at around 200 mM KCl containing DHC were pooled and dialyzed into 20 mM potassium phosphate buffer (pH 7.5). The protein was loaded onto a hydroxyapatite column pre-equilibrated with 20 mM potassium phosphate buffer (pH 7.5) and eluted using a 20 to 500 mM potassium phosphate gradient. The final step involved gel filtration over a Sephadex G 50 column in 100 mM Tris-HCl (pH 7.5) and resulted in a protein which appears as a single band on a SDS−PAGE gel.

Purification of SHP was as follows. *E. coli* cells were disrupted by ultrasonication in 10 mM Tris-HCl (pH 7.2) and 1 mM EDTA, in the presence of PMSF. Cell debris was removed by centrifugation at 18000*g* for 30 min. SHP was then loaded onto a DE-52 anion exchange column equilibrated with 10 mM Tris-HCl (pH 7.2) and 1 mM EDTA. SHP bound to the column and was eluted at 120 mM KCl. After dialysis against 10 mM Tris-HCl (pH 7.2) and 1 mM EDTA, the protein was loaded onto a Q-Sepharose column connected to an ÄKTA FPLC system. Protein was eluted using a 0 to 300 mM KCl gradient, and fractions containing SHP were concentrated by centrifugation (Amicon Cen-

Table 1: Data Collection and Refinement Statistics for Native DHC

	λ_1	λ_2	λ_3
wavelength (Å)	0.931	1.740	1.736
resolution limit (Å)	30−1.85 (1.9−1.85)	30−3.2 (3.3−3.2)	30−3.2 (3.3−3.2)
no. of unique reflections	13408	4876	4872
redundancy	4.2	5.8	5.8
completeness (%)	95.2 (94.3)	98.0 (97.9)	98.0 (97.8)
$I/[\sigma(I)]$	11.4 (2.8)	23.6 (8.8)	23.2 (8.4)
R_{merge} (%)[a]	6.8 (34.2)	5.7 (9.3)	5.7 (9.4)
R_{cullis} (centric/acentric)	−	0.65/0.60	0.56/0.55
R_{cullis} (anomalous)	0.83	0.83	0.47
phasing power	−	1.35/1.93	1.63/2.17
figure of merit	0.58		
R_{cryst}/R_{free} (%)[b]	15.2/19.3		
average B (Å^2)	19.9		
rmsd for bond lengths (Å)	0.017		
rmsd for bond angles (deg)	1.59		

[a] $R_{merge} = \sum_h\sum_i|I(h) - I_I(h)|/\sum_h\sum_i I_I(h)$, where $I_I(h)$ and $I(h)$ are the ith and mean measurements of reflection h, respectively. [b] $R_{cryst} = \sum_h|F_o - F_c|/\sum_h F_o$, where F_o and F_c are the observed and calculated structure factor amplitudes of reflection h, respectively. R_{free} is the test reflection data set, 5% selected randomly for cross validation during crystallographic refinement.

Table 2: Data Collection and Refinement Statistics for Recombinant DHC

resolution (Å)	24.0−2.0
total no. of reflections	109365
no. of unique reflections	9175
completeness (%)	97.6
$I/[\sigma(I)]$	10.8
R_{merge} (%)[a]	6.9
R_{merge} in the outer shell (2.07−2.00 Å) (%)	16.9
R_{cryst}/R_{free} (%)[b]	17.1/21.0
rmsd for bond lengths (Å)	0.021
rmsd for bond angles (deg)	1.94
Ramachandran analysis	
most favored (%)	88.1
additionally allowed (%)	11.9

[a] $R_{merge} = \sum_h\sum_i|I(h) - I_I(h)|/\sum_h\sum_i I_I(h)$, where $I_I(h)$ and $I(h)$ are the ith and mean measurements of reflection h, respectively. [b] $R_{cryst} = \sum_h|F_o - F_c|/\sum_h F_o$, where F_o and F_c are the observed and calculated structure factor amplitudes of reflection h, respectively. R_{free} is the test reflection data set, 5% selected randomly for cross validation during crystallographic refinement.

triprep, 10 kDa molecular mass cutoff) prior to further purification by size exclusion chromatography. This was performed using a Superdex 75 column with 10 mM Tris-HCl (pH 7.2) and 10 mM EDTA. Eluted SHP was concentrated by centrifugation and stored at −20 °C until it was required. The yield of pure SHP (running as a single band on a SDS−PAGE gel) obtained was approximately 1 mg per liter of *E. coli* culture.

Crystal Structure Determination of Native and Heterologously Expressed Recombinant DHC. Native protein was purified from *R. sphaeroides* as described previously (*11*). Crystals were obtained by the hanging-drop vapor diffusion method, using 20% PEG 3000, 0.2 M ammonium acetate, and 0.1 M MES (pH 6.0) as the precipitant. Crystals were flash-cooled by being plunged in liquid nitrogen after brief immersion in the mother liquor supplemented with 10% PEG 200. The platelike crystals were found to belong to space group $P3_121$ with the following unit cell dimensions: $a = b = 72.8$ Å and $c = 51.5$ Å.

A native data set to 1.85 Å resolution, which was used as the remote data set ($\lambda_1 = 0.931$ Å) for MAD phasing and as a high-resolution data set for refinement, was collected at beamline BM30 at ESRF (Grenoble, France). Subsequently, diffraction data extending to 3.2 Å were collected at 1.740 Å (λ_2 = inflection) and 1.736 Å (λ_3 = peak). Measured intensities were integrated and scaled using the HKL package (*16*), and data statistics are given in Table 1. The CCP4 program package (*17*) was used to convert intensities to structure factors and to merge the scaled data sets.

The anomalous difference Patterson maps calculated from the λ_3 data set showed clear peaks from which the position of both expected Fe sites could be determined. The calculation of MAD phases and refinement of the Fe positions were carried out using all diffraction data for λ_1−λ_3 up to 2.8 Å. The occupancy and position of both Fe sites were refined using MLPHARE (*17*), converging to an overall figure of merit of 0.58 for the resolution range of 30−2.8 Å.

Experimental phases were extended to 1.85 Å using DM (*18*), and ARPWARP6.1 (*19*) was used to successfully trace the molecule and provide an initial model using the solvent flattening extended phases. Manual rebuilding cycles were carried out using TURBO-FRODO (*20*), alternating with maximum-likelihood-based refinement using REFMAC (*21*). Refinement statistics are given in Table 1.

Heterologously expressed recombinant DHC was crystallized using the hanging-drop vapor diffusion method at 18 °C using 25−30% PEG 8000, 0.1 M $MnSO_4$, and 0.1 M sodium cacodylate buffer (pH 6.5) as the precipitant. Drops were prepared by adding 200 μM protein {200 μM in both DHC and SHP [in 100 mM Tris-HCl buffer (pH 7.5)] in an attempt to cocrystallize these two proteins}. After ∼7 days, needles up to 2 mm in length were formed. Crystals were flash-cooled by being plunged in liquid nitrogen after brief immersion in mother liquor supplemented with 23% glycerol. Crystals were found to belong to space group $C2$ with the following cell dimensions: $a = 93.0$ Å, $b = 45.2$ Å, $c = 34.4$ Å, and $\beta = 105.9°$. A data set was collected at SRS Daresbury (station 14.1, $\lambda = 1.488$ Å) using an ADSC Quantum 4 detector. Data processing was carried out using the HKL package (*16*). From the calculated Matthews coefficient, it was apparent that the asymmetric unit contained only one molecule of one of the proteins present in the drop. Molecular replacement was carried out using the native DHC structure. Manual rebuilding cycles were carried out using TURBO-FRODO (*20*), alternating with maximum-likelihood-based refinement using REFMAC (*21*). Refinement statistics are given in Table 2. Structure factors and model coordinates have been deposited with the Protein Data Bank (entry 2FWT for *R. sphaeroides* purified DHC and entry 2FW5 for recombinant DHC).

Protein−Protein Interaction. To assess the interaction between SHP and DHC, two double cuvettes (2 × 1.5 mL capacity) and a double-beam UV−vis spectrophotometer (Shimadzu 2101) were used. In the reference cell, a DHC solution (8 μM) was prepared in buffer (10 mM HEPES at pH 7.2 and 25 °C) in one compartment, and SHP was added to buffer in small aliquots (1−2 μM) in the second compartment. In the observation cell, buffer only was added to one compartment, while SHP was added in small aliquots (1−2 μM) to DHC (8 μM) in the other compartment. The DHC concentration used was necessary to obtain spectral data of

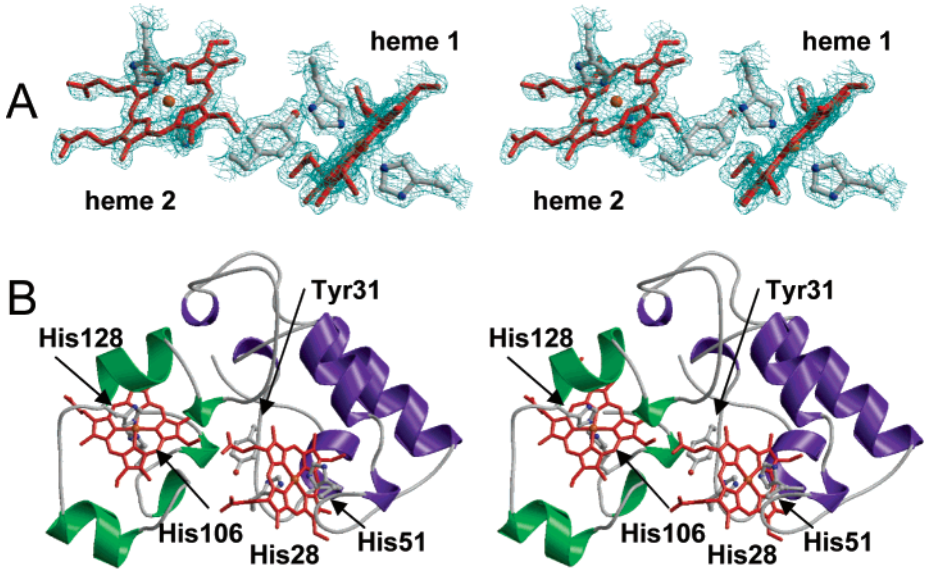

FIGURE 1: (A) Stereo representation of the electron density surrounding the heme groups, their histidine ligands, and Tyr31 of the recombinant DHC structure. The electron density map was calculated using Fourier coefficients $2F_o - F_c$, where F_o and F_c are the observed and calculated structure factors, respectively, the latter based on the final model. The contour level is 1.5σ, where σ is the rms electron density. (B) Stereo representation of the recombinant DHC structure. The individual domains are colored purple (N-terminal domain), green (C-terminal domain), and gray (linker polypeptide). The position of Tyr31 between the two heme groups can be seen clearly. This figure was generated using BOBSCRIPT (*31*) and RASTER 3D (*32*).

sufficient quality. Similar experiments were carried out at increasing ionic strengths (up to 500 mM) by the addition of KCl. The difference in absorption was plotted against SHP concentration and fitted to the equation $\Delta A = A_{max}(\{(S + E + K_d) \pm \sqrt{[(S + E + K_d)^2 - 4ES]}\}/2)$, where S is the SHP concentration, E is the DHC concentration, K_d is the dissociation constant, A_{max} is the maximum absorbance change, and ΔA is the change in absorbance.

OTTLE (Optically Transparent Thin Layer Electrode) Potentiometry. Spectroelectrochemical analyses of SHP and DHC were conducted in an OTTLE cell constructed from a modified quartz EPR cell with a path length of 0.3 mm, containing a Pt/Rh (95/5) gauze working electrode (wire diameter of 0.06 mm, mesh size of 1024 cm^{-1}, Engelhardt), a platinum wire counter electrode, and a Ag/AgCl reference electrode (model MF2052, Bioanalytical Systems). Protein samples (0.5 mL at 100−200 μM) were eluted through a Sephadex G-25 column pre-equilibrated with 0.1 M Tris-HCl (pH 7.5) and 0.5 M KCl, in an anaerobic glovebox. Depending on the expected midpoint potential, an appropriate selection of the following mediators was added: phenazine ethosulfate, phenazine methosulfate, 2-hydroxy-1,4-naphthoquinone, pyocyanine, benzyl viologen, methyl viologen (all at 20 μM), and FMN (5 μM). Spectroelectrochemical titrations were performed at 25 ± 2 °C using an Autolab PGSTAT10 potentiostat and a Cary 50 UV−vis spectrophotometer. The potential of the working electrode was decreased in 30 mV steps until the protein was fully reduced and increased stepwise until reoxidation was complete. After each step, the current and UV−vis absorption spectra were monitored until no further change occurred. This equilibration process typically lasted 10 min. Absorbance changes were plotted against the potential of the working electrode and analyzed using the Nernst equation. The Ag/AgCl reference electrode employed in the OTTLE cell was calibrated against indigotrisulfonic acid (E_m = −99 mV vs SHE) and FMN (E_m = −220 mV vs SHE) under the same buffer conditions. All electrode potentials were corrected accordingly by 200 ± 2 mV relative to the standard hydrogen electrode.

Kinetic Analyses. Anaerobic stopped-flow spectrophotometry was performed using an Applied Photophysics SX.17MV stopped-flow spectrophotometer contained within a Belle Technology glovebox with an oxygen concentration maintained below 5 ppm. All experiments were carried out in degassed buffer [20 mM Tris-HCl (pH 7.2) and 500 mM KCl] at 10 °C, and all measurements were obtained using either single-wavelength or diode-array detectors.

Kinetics of electron transfer from reduced DHC to oxidized SHP was determined as follows. Reduced DHC (excess dithionite removed by gel filtration) of varying concentration (up to 15 μM) was mixed with oxidized SHP (≤2 μM). The reaction was monitored at 431 nm over a 10−200 ms time scale.

The kinetics of formation of the oxy−ferrous SHP complex was monitored at 421 nm on a 100−200 ms time scale. Reduced SHP (2 μM, excess dithionite removed) was mixed with buffer containing various concentrations of dissolved oxygen (65−260 μM). The rate of decay of the oxy−ferrous SHP complex was followed over a 3 h period, at the same wavelength.

The composite interaction of SHP, DHC, and O_2 was examined in the following way. Reduced DHC (20 μM) was mixed with oxidized SHP (20 μM) in oxygenated buffer (260 μM in O_2). The reaction was monitored at 400−700 nm at time periods of 1, 16, 32, 65, and 2100 s. High protein concentrations were used so that changes in the α and β peaks could be monitored accurately. This was necessary because the DHC and SHP spectra overlap in the Soret region.

RESULTS AND DISCUSSION

Crystal Structures of DHC. The crystal structure of recombinant DHC (*C*2 space group) consists of residues

Ala12−Phe136 (the first 11 and the last residue had no discernible electron density and were therefore omitted from the model), two heme groups, and 92 water molecules. In contrast, the native DHC crystallized in the $P3_121$ space group and lacked residues 80−91 in addition to the first 11 residues and the C-terminal residue. This was clearly a result of limited proteolysis occurring prior to crystallization as the $P3_121$ crystal packing does not provide space for the polypeptide segment connecting residues 79 and 92. As a consequence of limited proteolysis and different crystal packing, minor differences in both backbone and side chain positions are observed between both DHC structures. The following structure description and comparison is based on the recombinant DHC structure unless stated otherwise.

The 16 kDa DHC folds into two distinct domains, each binding a single heme group and connected by a small linker region (Figure 1). Despite little sequence similarity, the N-terminal domain (residues 12−75) clearly belongs to the cytochrome *c* class I family and is structurally most similar to the cytochrome *c* domains and/or subunits of flavocytochrome *p*-cresol methylhydroxylase [PDB entry 1DII (*22*), *Z* score of 3.9 for 53 Cα atoms using Dali (*23*)] and sulfite dehydrogenase [PDB entry 2BLF (*24*), *Z* score of 6.4 for 59 Cα atoms using Dali]. In contrast to the latter, the N-terminal heme of DHC is axially ligated by two histidines (His28 and His51) rather than the more classical His-Met ligation. The C-terminal domain (residues 94−136) displays no significant similarity to any structure presently available and thus constitutes a novel *c*-type heme binding structural motif. Like the majority of cytochrome *c* structures, this domain consists entirely of α-helical and connecting loop segments. The covalently bound heme is coordinated axially by two nearly perpendicularly oriented histidines (His128 and His106) and is markedly more solvent-exposed (171 Å^2) than the N-terminal heme (102 Å^2). A large part of the C-terminal hydrophobic heme binding pocket is in fact lined by residues from the N-terminal domain. Taken together with the small amino acid:heme ratio of 42:1, it is unlikely that the C-terminal domain could exist as an independent folding unit. Most low-molecular mass diheme cytochrome *c* structures contain a closely interacting pair of nearly parallel oriented hemes [e.g., NapB (*25*) and DHC2 (*26*)], but in DHC, the hemes are not in van der Waals contact. The smallest edge-to-edge distance between the aromatic heme moieties is 10.2 Å, leaving a gap that is filled predominantly by the aromatic Tyr31. This arrangement of heme cofactors distantly resembles that of diheme flavocytochrome FCSD [PDB entry 1FCD (*27*)] and related structures.

Protein−Protein Interactions and Kinetics of Electron Transfer from DHC to SHP. SHP and DHC bind very tightly, with a K_d of 0.26 ± 0.05 μM (10 mM HEPES at pH 7.2 and 25 °C). This is shown in Figure 2. At increasing salt concentrations, the binding becomes weaker (K_d = 1.0 ± 0.2 μM at I = 200 mM KCl), and at high ionic strengths, protein−protein binding is nonspecific and data can no longer be fitted accurately. It is therefore clear that SHP and DHC bind very effectively at lower ionic strengths, suggesting a strong electrostatic interaction.

Measurement of the electron transfer kinetics between the two proteins was carried out using stopped-flow methods, mixing reduced DHC with oxidized SHP, and monitoring the reaction at 431 nm. At room temperature and lower KCl concentrations (e.g., <200 mM), electron transfer occurs too quickly to be measured by stopped-flow methods. Only at higher salt concentrations (500 mM KCl) and a low temperature (10 °C) could an accurate result be obtained. The resultant rate constant (k) for electron transfer from reduced DHC to oxidized SHP was found to be (1.8 ± 0.1) × 10^7 M^{-1} s^{-1}, indicating very efficient interprotein electron transfer. This is illustrated in Figure 3.

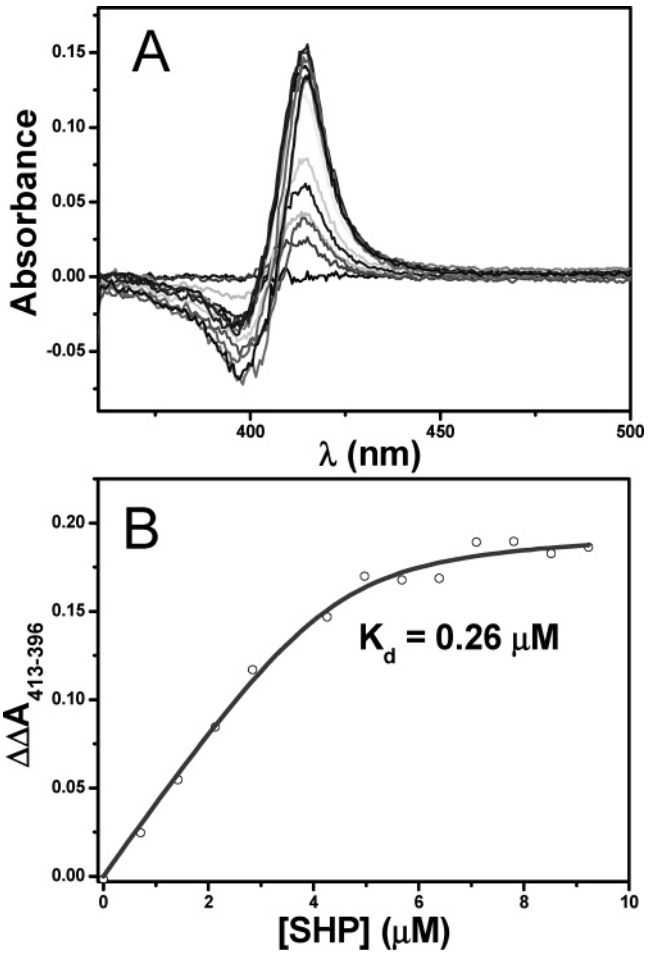

FIGURE 2: (A) Difference spectra of physically added compared to spectrally added SHP to DHC (10 mM HEPES at pH 7.2 and 25 °C). (B) Difference in the change of absorbance plotted vs the concentration of SHP added. This is fitted to the equation $\Delta A = A_{max}(\{(S + E + K_d) \pm \sqrt{[(S + E + K_d)^2 - 4ES]}\}/2)$, from which the dissociation constant can be obtained.

Redox Potentiometry of SHP and DHC. The midpoint potential of SHP (determined by potentiometric titration) was previously reported to be −22 mV (*1*). This potential has been redetermined using the OTTLE method. The absorbance change at 426 nm in the SHP spectrum accurately reflects the change in the heme reduction state. This can be seen in Figure 4, along with a plot of the proportion of protein reduced against measured potential. These data fit to a one-electron Nernst curve, resulting in a reduction potential for the SHP heme of −105 ± 5 mV. The reduction and reoxidation of SHP are fully reversible, even though SHP has a labile sixth ligand to the heme iron.

For the DHC experiment, the absorption at 552 nm was used as an indicator of protein reduction since it gave the clearest spectral changes. The spectral changes observed during the titration are shown in Figure 5A. Figure 5B shows a plot of the proportion of protein reduced against measured

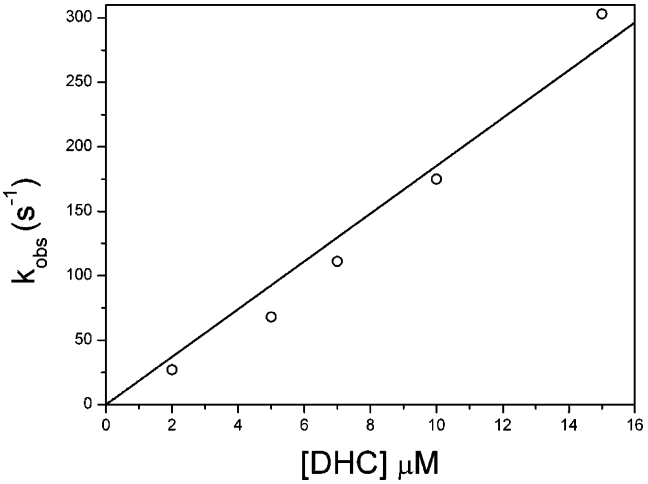

FIGURE 3: Kinetics of electron transfer from DHC to SHP (500 mM KCl in 20 mM Tris-HCl at pH 7.2 and 10 °C). Observed rates were plotted vs the concentration of DHC. The gradient provides the second-order rate constant for the reaction.

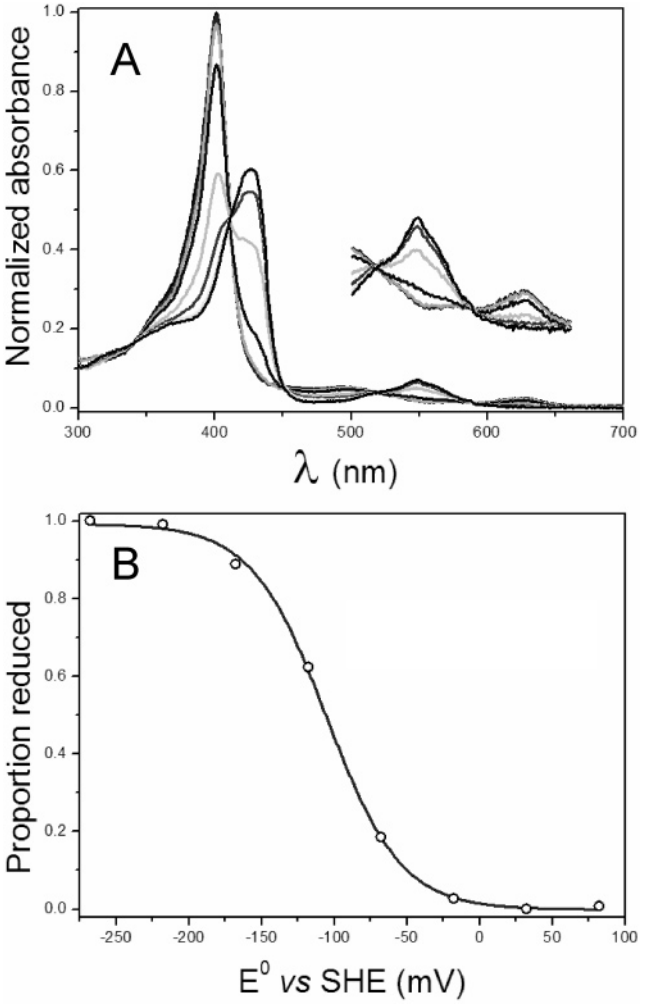

FIGURE 4: (A) Spectral shifts observed during stepwise electrochemical reduction of SHP. The lines represent spectra collected at various stages during the reduction. (B) Proportion of SHP reduced plotted vs the reduction potential, fitted to a one-electron Nernst function.

potential. These data fit to a two-times-one-electron Nernst curve and yield midpoint reduction potentials of -240 ± 5 and -310 ± 5 mV. As in the case of SHP, the reduction

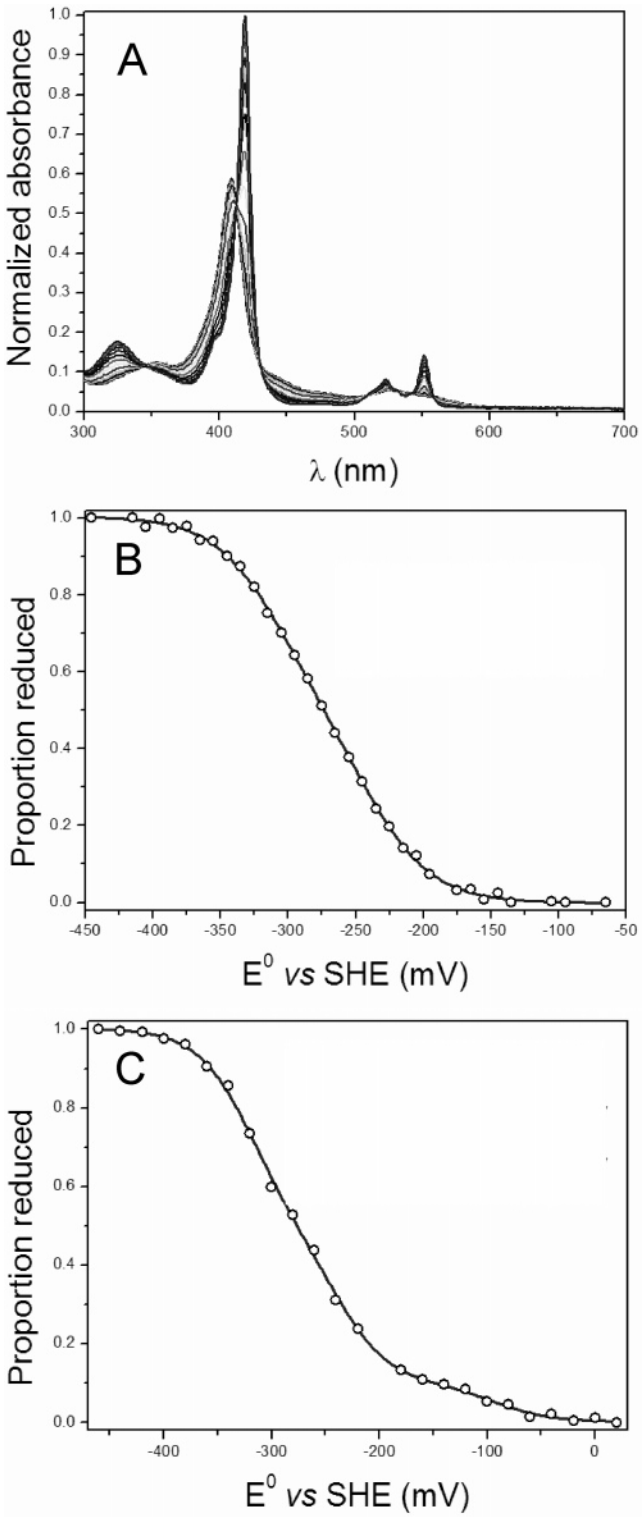

FIGURE 5: (A) Spectral shifts observed during stepwise electrochemical reduction of DHC (0.5 mM KCl in 0.1 mM Tris-HCl at pH 7.5 and 25 °C). The lines represent spectra collected at various stages during the reduction. (B) Proportion of DHC reduced vs the reduction potential, fitted to a two-times-one-electron Nernst function. (C) Proportion of the reduced complex vs the reduction potential, fitted to a two-times-one-plus-one-electron Nernst function.

and reoxidation are freely reversible with no observed hysteresis.

In addition to the separate measurement of the midpoint potentials of the two proteins, an OTTLE experiment was carried out to determine the potentials of the proteins in a

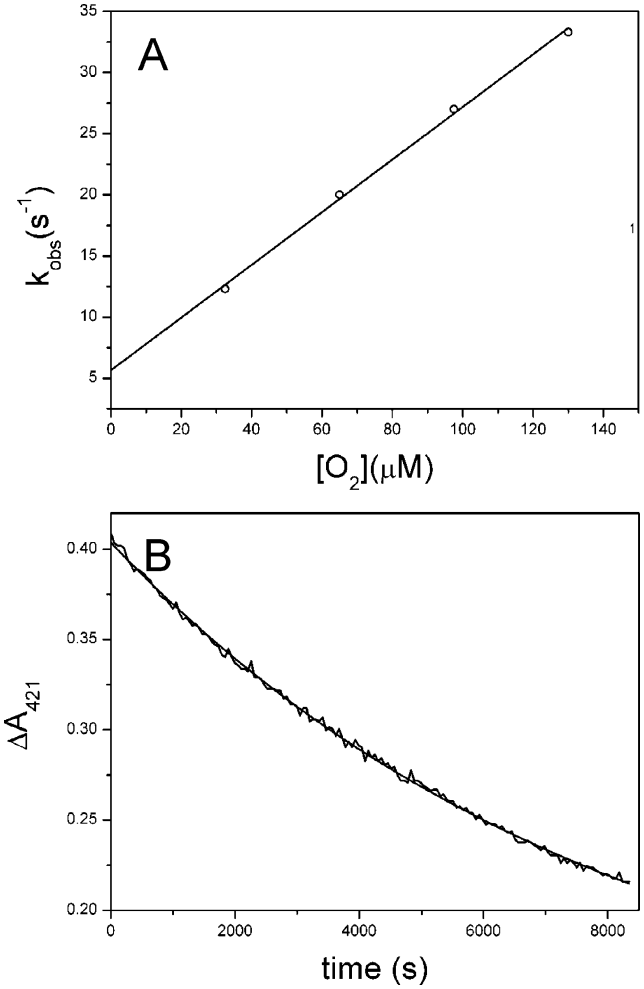

FIGURE 6: (A) Kinetics of binding of oxygen to ferrous SHP (20 mM Tris-HCl, 500 mM KCl, pH 7.2, and 10 °C). (B) Kinetics of the decay of the oxy−ferrous SHP complex (20 mM Tris-HCl, 500 mM KCl, pH 7.2, and 10 °C). Data have been fitted to a single exponential to give a first-order rate constant.

SHP−DHC complex. To prevent perturbation of complex formation, this experiment was carried out under conditions with an ionic strength lower than that for the isolated proteins, at 100 mM KCl rather than 500 mM KCl. By monitoring the absorbance change at 419 nm, we were able to obtain the data shown in Figure 5C. It can be seen that these data may be fitted to a two-times-one-plus-one-electron Nernst curve, with potentials of -92 ± 12, -238 ± 6, and -320 ± 5 mV. These values are, within error, the same as those measured for the proteins independent of each other. This is consistent with the heme potentials being unaltered upon complex formation.

Kinetics of Formation and Decay of the Oxy−Ferrous SHP Complex. Figure 6A shows the rate of formation of the oxy−ferrous form of SHP. The association rate constant (k_{on}) is $(2.21 \pm 0.06) \times 10^5$ M^{-1} s^{-1}, which is comparable to that of NO binding (unpublished observations). This could suggest that the SHP heme-binding site is optimized for accommodation of bent diatomics. In contrast to NO binding, however, the oxy−ferrous complex has a measurable dissociation rate constant (k_{off}) of 5.7 ± 0.6 s^{-1}. From this, we can calculate a dissociation constant (K_d) of 26 ± 3 μM. This value is of interest as it is similar to those of the oxygen-sensing proteins *Rm*FixL (*28*), *Ec*Dos (*29*), and *Ax*PDEA1 (*30*).

Figure 6B shows the rate of decay of the oxy−ferrous SHP complex. Although in air the half-life of the oxy−ferrous species is only 3 min, under anaerobic conditions it is appreciably more stable. At 10 °C, the half-life of its decay back to ferric heme, probably via the dissociation of superoxide, is 1.6 h [$k_{dec} = (1.23 \pm 0.2) \times 10^{-3}$ s^{-1}]. Even at room temperature, the half-life is still 10 times that in air [0.17 h, $k_{dec} = (1.1 \pm 0.1) \times 10^{-3}$ s^{-1}]. It is possible that this stability could also point toward an oxygen-sensing role for SHP.

DHC, SHP, O_2 System. Although it is clear that DHC transfers electrons rapidly to SHP, it is unclear whether SHP displays any enzymatic activity in the presence of DHC and an exogenous ligand. For example, it is possible that DHC might be required to provide more than one electron to SHP to reduce a substrate. Because of the moderate dissociation constant for oxygen binding and the stability of the oxy−ferrous form of SHP, O_2 was chosen as a possible substrate. Mixing of reduced DHC with oxidized SHP in a 1:1 ratio in oxygenated buffer led to very complex spectra incorporating a number of different processes occurring over similar time scales. These include the reduction of SHP by DHC, the formation and decay of the SHP oxy−ferrous complex, and the reoxidation of DHC. By careful identification of the isosbestic points for each of the possible reactions, the rate of each process could be deciphered using Global Analysis. Figure 7 shows example stopped-flow traces over varying time spans (1, 16, 65, and 2100 s).

Starting from the fastest process, we show in panel A the spectral changes accompanying one-electron transfer from DHC to SHP and subsequent formation of the SHP oxy−ferrous complex. At 532 nm, DHC displays an isosbestic point, allowing reduction of SHP, and formation of its oxy−ferrous complex, to be observed. Fitting the absorbance change at 532 nm versus time gives first-order rate constants for DHC to SHP electron transfer and SHP oxy−ferrous complex formation of 340 ± 30 and 12.0 ± 1.3 s^{-1}, respectively. Panel B shows the start of the process of removal of the second electron from DHC, as well as the binding of oxygen to reduced SHP. At 570 nm, the wavelength at which a characteristic peak of the SHP oxy−ferrous complex appears, a sharp increase in absorbance, followed by a smaller increase in absorbance, could be seen. This corresponds to the binding of oxygen to reduced SHP and the complete reoxidation (i.e., loss of the second electron) of DHC, respectively. Fitting the absorbance at 570 nm versus time gives rise to the first-order rate constant for each process. These were 0.040 ± 0.006 s^{-1} for the removal of the second electron from DHC and 12.0 ± 0.3 s^{-1} for the formation of the SHP oxy−ferrous complex. Panel C also shows the removal of the second electron from DHC, as evidenced by the large decrease in absorbance at 551.5 nm, a characteristic peak in the spectrum of reduced DHC. However, the wavelengths at which the data could best be fitted (as close as possible to the SHP isosbestic points) were 524 and 568 nm. The first-order rate constant was therefore determined by fitting the change in absorbance at these wavelengths versus time, with each fit giving a value of 0.040 ± 0.006 s^{-1}, in agreement with the rate constant determined from panel B. Finally, panel D shows reoxidation of the oxy−ferrous SHP complex to oxidized SHP. This is indicated by the slow increases in absorbance at 627 nm, a charac-

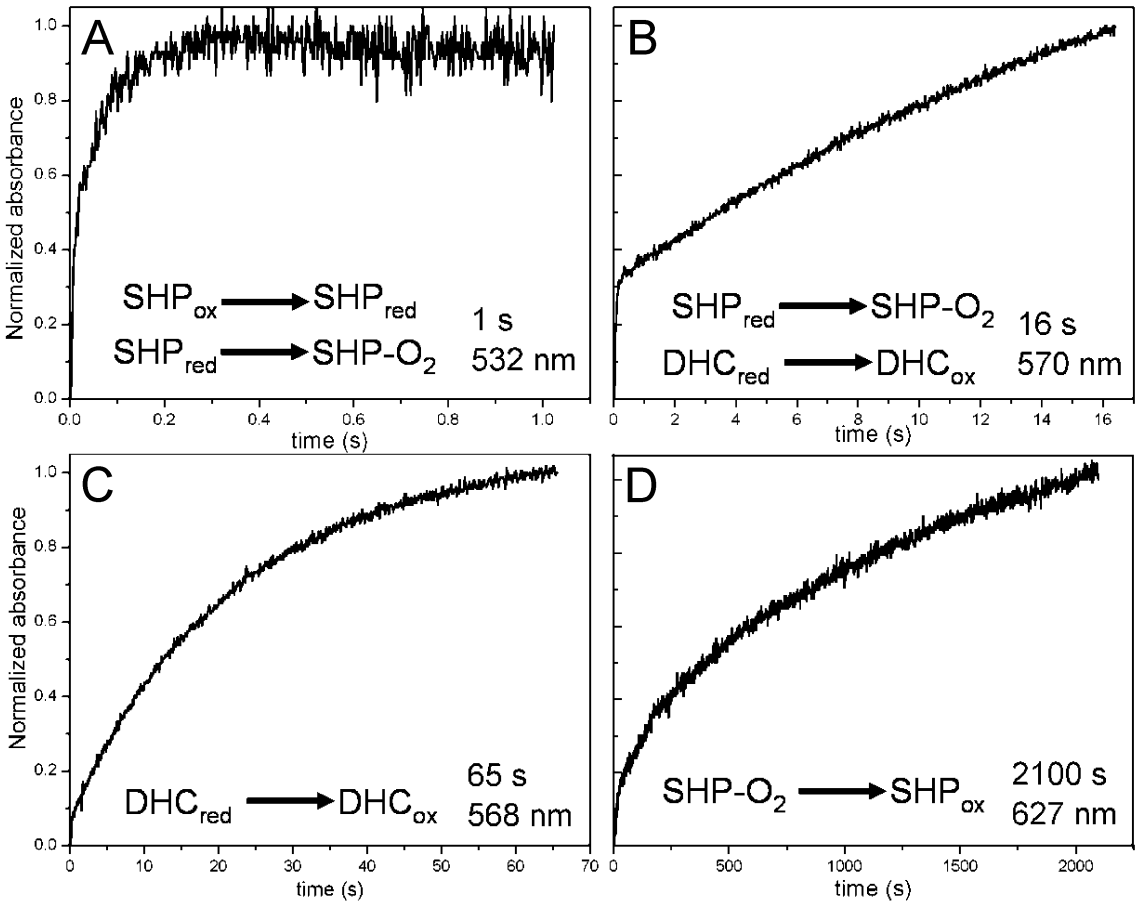

FIGURE 7: Example stopped-flow traces over each time scale [1 (A) 16 (B), 65 (C), and 2100 s (D)] for the $DHC_{red} + SHP_{ox} + O_2$ reaction, carried out in 20 mM Tris-HCl at pH 7.2 and 10 °C. The processes occurring in each trace are indicated. Traces were analyzed using Global Analysis, which can fit overlapping reaction steps with their corresponding rate constant (fits not shown).

Table 3: First-Order Rate Constants for Each Step of the DHC + SHP + O_2 Reaction (20 mM Tris-HCl, pH 7.2, 500 mM KCl, and 10 °C)

step	first-order rate constant (s^{-1})
$SHP_{ox} \rightarrow SHP_{red}$	340 ± 30
$SHP_{red} \rightarrow SHP{-}O_2$	12 ± 1.3
$DHC_{red} \rightarrow DHC_{ox}$	0.04 ± 0.006
$SHP{-}O_2 \rightarrow SHP_{ox}$	0.001 ± 0.0005

teristic peak of the oxidized SHP spectrum. Fitting the change in absorbance at 627 nm versus time, a first-order rate constant of $(1.0 \pm 0.5) \times 10^{-3}$ s^{-1} is obtained. These data are summarized in Table 3. From the data obtained, it is clear that the rates measured in the SHP, DHC, O_2 combined system differ little from those measured separately. Thus, when DHC is introduced into the system, no O_2 turnover by SHP is observed.

Related Systems. In all cases, the operon encoding SHP also encodes DHC and a membrane-bound cytochrome *b*. However, the organization of these and other associated genes is somewhat variable. In *R. sphaeroides*, only three genes are found in the cluster, encoding SHP, DHC, and a fusion of cytochrome *b* with a second DHC that is 45% identical to the soluble protein described in this paper. The homologous region of the *S. oneidensis* genome (*6*) reveals an additional three reading frames that correspond to a conserved hypothetical protein (SO4486), a DNA-binding response regulator (SO4487), and a sensor histidine kinase (SO4488). The presence of regulatory proteins in the SHP operons of this and several other organisms substantiates the idea that SHP could function as a sensor, possibly for oxygen. The hypothesis that SHP may be operating as an oxygen sensor arises from the oxygen binding characteristics of the protein, and in particular the stability of the SHP oxy−ferrous complex.

From the available evidence, the role of SHP is as yet unclear. Although we have demonstrated that SHP is readily reduced by DHC, we cannot be certain that this represents a physiological respiratory chain, or indeed what the electron acceptor in such a chain may be. To address this question, we aim to carry out phenotype studies with gene knockouts.

CONCLUSIONS

In this work, we present the crystal structure of DHC to 1.85 Å resolution, and this indicates the presence of a structurally unique domain around one of the heme groups. In addition, we provide evidence of complementary binding, favorable midpoint potentials, and efficient electron transfer in the DHC−SHP system. This represents evidence for the possible operation of DHC and SHP as physiological partners. It is likely that the DHC−SHP interaction is electrostatic in nature.

ACKNOWLEDGMENT

We are very grateful to Katrien Backers for providing assistance with the heterologous overproduction of DHC and

SHP in *E. coli* and to Terry Meyer for assistance in purification of DHC from *R. sphaeroides*.

REFERENCES

1. Meyer, T. E., and Cusanovich, M. A. (1985) Soluble cytochrome composition of the purple phototrophic bacterium, *Rhodopseudomonas sphaeroides* ATCC 17023, *Biochim. Biophys. Acta 807*, 308−319.
2. Monson, E. K., Weinstein, M., Ditta, G. S., and Helinski, D. R. (1992) The FixL protein of *Rhizobium meliloti* can be separated into a heme-binding oxygen-sensing domain and a functional C-terminal kinase domain, *Proc. Natl. Acad. Sci. U.S.A. 89*, 4280−4284.
3. Aono, S. (2003) Biochemical and Biophysical Properties of the CO-Sensing Transcriptional Activator CooA, *Acc. Chem. Res. 36*, 825−831.
4. Rodgers, K. R. (1999) Heme-based sensors in biological systems, *Curr. Opin. Chem. Biol. 3*, 158−167.
5. Leys, D., Backers, K., Meyer, T. E., Hagen, W. R., Cusanovich, M. A., and Van Beeumen, J. J. (2000) Crystal structures of an oxygen-binding cytochrome *c* from *Rhodobacter sphaeroides*, *J. Biol. Chem. 275*, 16050−16056.
6. Heidelberg, J. F., Paulsen, I. T., Nelson, K. E., Gaidos, E. J., Nelson, W. C., Read, T. D., Eisen, J. A., Seshadri, R., Ward, N., Methe, B., Clayton, R. A., Meyer, T., Tsapin, A., Scott, J., Beanan, M., Brinkac, L., Daugherty, S., DeBoy, R. T., Dodson, R. J., Durkin, A. S., Haft, D. H., Kolonay, J. F., Madupu, R., Peterson, J. D., Umayam, L. A., White, O., Wolf, A. M., Vamathevan, J., Weidman, J., Impraim, M., Lee, K., Berry, K., Lee, C., Mueller, J., Khouri, H., Gill, J., Utterback, T. R., McDonald, L. A., Feldblyum, T. V., Smith, H. O., Venter, J. C., Nealson, K. H., and Fraser, C. M. (2002) Genome sequence of the dissimilatory metal ion-reducing bacterium *Shewanella oneidensis*, *Nat. Biotechnol. 20*, 1118−1123.
7. www.jgi.doe.gov.
8. Coenye, T., and Vandamme, P. (2003) Diversity and significance of *Burkholderia* species occupying diverse ecological niches, *Environ. Microbiol. 5*, 719−729.
9. Achenbach, L. A., Michaelidou, U., Bruce, R. A., Fryman, J., and Coates, J. D. (2001) *Dechloromonas agitata* gen. nov., sp. nov. and *Dechlorosoma suillum* gen. nov., sp. nov., two novel environmentally dominant (per)chlorate-reducing bacteria and their phylogenetic position, *Int. J. Syst. Bacteriol. 51*, 527−533.
10. Salama, S. M., Newnham, E., Chang, N., and Taylor, D. E. (1995) Genome map of *Campylobacter fetus* subsp. *fetus* ATCC 27374, *FEMS Microbiol. Lett. 132*, 239−245.
11. Vandenberghe, I., Leys, D., Demol, H., Van Driessche, G., Meyer, T. E., Cusanovich, M. A., and Van Beeumen, J. J. (1998) The primary structures of the low-redox potential diheme cytochromes *c* from the phototrophic bacteria *Rhodobacter sphaeroides* and *Rhodobacter adriaticus* reveal a new structural family of *c*-type cytochromes, *Biochemistry 37*, 13075−13081.
12. http://bccm.belspo.be/db/lmbp_plasmid_details.php?NM = pMc519.
13. Thöny-Meyer, L. (2000) Haem-polypeptide interactions during cytochrome *c* maturation, *Biochim. Biophys. Acta 1459*, 316−324.
14. Backers, K. (2000) Ph.D. Thesis, University of Ghent, Ghent, Belgium.
15. De Sutter, K., Hostens, K., Vandekerckhove, J., and Fiers, W. (1994) Production of enzymatically active rat protein disulfide isomerase in *Escherichia coli*, *Gene 141*, 163−170.
16. Otwinowski, Z., and Minor, W. (1997) Processing of X-ray diffraction data collected in oscillation mode, *Methods Enzymol. 276*, 307−326.
17. Collaborative Computational Project, Number 4 (1994) The CCP4 Suite: Programs for Protein Crystallography, *Acta Crystallogr. D50*, 760−763.
18. Cowtan, K. (1994) 'dm': An automated procedure for phase improvement by density modification, *Joint CCP4 and ESF-EACBM Newsletter on Protein Crystallography 31*, 34−38.
19. Lamzin, V. S., Perrakis, A., and Wilson, K. S. (2001) The ARP/wARP suite for automated construction and refinement of protein models, in *International Tables for Crystallography. Volume F: Crystallography of biological macromolecules* (Rossmann, M. G., and Arnold, E., Eds.) pp 720−722, Kluwer Academic Publishers, Dordrecht, The Netherlands.
20. Roussel, A., and Cambillau, C. (1991) TURBO-FRODO, in *Silicon Graphics Geometry Partners Directory 86*, Silicon Graphics, Mountain View, CA.
21. Murshudov, G. N., Vagin, A. A., and Dodson, E. J. (1997) Refinement of macromolecular structures by the maximum-likelihood method, *Acta Crystallogr. D53*, 240−255.
22. Cunane, L. M., Chen, Z. W., Shamala, N., Mathews, F. S., Cronin, C. N., and Mcintire, W. S. (2000) Structures of the flavocytochrome *p*-cresol methylhydroxylase and its enzyme−substrate complex: Gated substrate entry and proton relays support the proposed catalytic mechanism, *J. Mol. Biol. 295*, 357−374.
23. Holm, L., and Sander, C. (1998) Touring protein fold space with Dali/FSSP, *Nucleic Acids Res. 26*, 316−319.
24. Kappler, U., and Bailey, S. (2005) Molecular basis of intramolecular electron transfer in sulfite-oxidizing enzymes is revealed by high-resolution structure of a heterodimeric complex of the catalytic molybdopterin subunit and a *c*-type cytochrome subunit, *J. Biol. Chem. 280*, 24999−25007.
25. Brige, A., Leys, D., Meyer, T. E., Cusanovich, M. A., and Van Beeumen, J. J. (2002) The 1.25 Å resolution structure of the diheme NapB subunit of soluble nitrate reductase reveals a novel cytochrome *c* fold with a stacked heme arrangement, *Biochemistry 41*, 4827−4836.
26. Heitmann, D., and Einsle, O. (2005) Structural and biochemical characterization of DHC2, a novel diheme cytochrome *c* from *Geobacter sulfurreducens*, *Biochemistry 44*, 12411−12419.
27. Chen, Z.-w., Koh, M., Van Driessche, G., Van Beeumen, J. J., Bartsch, R. G., Meyer, T. E., Cusanovich, M. A., and Mathews, F. S. (1994) The structure of flavocytochrome *c* sulfide dehydrogenase from a purple phototrophic bacterium, *Science 266*, 430−432.
28. Gilles-Gonzalez, M. A., Gonzalez, G., Perutz, M. F., Kiger, L., Marden, M. C., and Poyart, C. (1994) Heme-based sensors, exemplified by the kinase FixL, are a new class of heme protein with distinctive ligand binding and autoxidation, *Biochemistry 33*, 8067−8073.
29. Delgado-Nixon, V. M., Gonzalez, G., and Gilles-Gonzalez, M. A. (2000) Dos, a heme-binding PAS protein from *Escherichia coli*, is a direct oxygen sensor, *Biochemistry 39*, 2685−2691.
30. Chang, A. L., Tuckerman, J. R., Gonzalez, G., Mayer, R., Weinhouse, H., Volman, G., Amikam, D., Benzimam, M., and Gilles-Gonzalez, M. A. (2001) Phosphodiesterase A1, a regulator of cellulose synthesis in *Acetobacter xylinum*, is a heme-based sensor, *Biochemistry 40*, 3420−3426.
31. Esnouf, R. M. (1997) An extensively modified version of MolScript that includes greatly enhanced coloring capabilities, *J. Mol. Graphics 15*, 132−134.
32. Merritt, E. A., and Murphy, M. E. P. (1994) *Raster3D*, version 2.0. A program for photorealistic molecular graphics, *Acta Crystallogr. D50*, 869−873.

BI060288Q